---

**Article:**
Prehm, M., Enders, C., Mang, X. et al. (5 more authors) (2018) Lamellar Liquid Crystals of In-Plane Lying Rod-Like Mesogens with Designer Side-Chains: the Case of Sliding vs Locked Layers. Chemistry, 24 (60). pp. 16072-16084.

https://doi.org/10.1002/chem.201802050

---

CHEMISTRY
A European Journal

A Journal of
ChemPubSoc Europe

## Accepted Article

**Title:** Lamellar Liquid Crystals of In-Plane Lying Rod-Like Mesogens with Designer Side-Chains: the Case of Sliding vs Locked Layers

**Authors:** Marko Prehm, Claudia Enders, Xiaobin Mang, Xiangbing Zeng, Feng Liu, Goran Ungar, Ute Baumeister, and Carsten Tschierske



**To be cited as:** *Chem. Eur. J.* 10.1002/chem.201802050

**Link to VoR:** http://dx.doi.org/10.1002/chem.201802050

Supported by
ACES

WILEY-VCH

10.1002/chem.201802050

# Lamellar Liquid Crystals of In-Plane Lying Rod-Like Mesogens with Designer Side-Chains: the Case of Sliding vs Locked Layers

Marko Prehm,[a] Claudia Enders, [a] Xiaobin Mang, [b] Xiangbing Zeng, [b] Feng Liu,*[c] Goran Ungar*[b,d] Ute Baumeister[a] and Carsten Tschierske*[a]

Dr. M. Prehm, Dr. C. Enders, Dr. U. Baumeister, Prof. Dr. C. Tschierske
Institute of Chemistry, Martin Luther University Halle-Wittenberg,
Kurt-Mothes-Str.2, D-06120 Halle, Germany.
e-mail: Carsten.tschierske@chemie.uni-halle.de

[b] Dr. X. Mang, Dr. X. Zeng, Prof. Dr. G. Ungar
Department of Engineering Materials, University of Sheffield,
Robert Hadfield Building Mappin Street, Sheffield S1 3JD, Great Britain.

[c] Prof. Dr. F. Liu
State Key Laboratory for Mechanical Behavior of Materials, Xi'an Jiaotong University,
Xi'an 710049, P. R. China

[d] Prof. Dr. G. Ungar
Department of Physics, Zhejiang Sci-Tech University,
Xiasha College Park, Hangzhou 310018, P. R. China

## Graphical Abstract

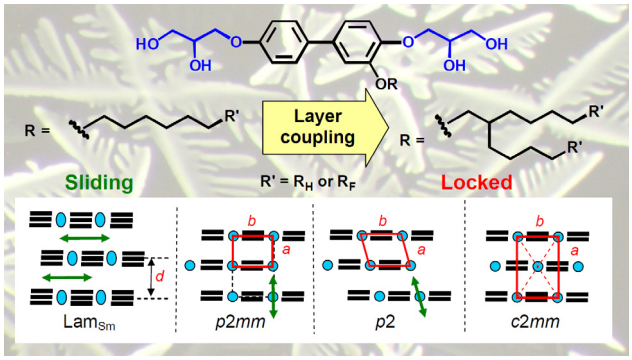

10.1002/chem.201802050

**Abstract**: The dimensionality of self-assembled nano-structures plays an essential role for their properties and applications. Here we provide an understanding of the transition from weakly to strongly coupled lamellea in soft matter systems involving in-plane organized π-conjugated rods. For this purpose bolaamphiphilic triblock molecules consisting of a rigid biphenyl core, polar glycerol groups at the ends, and a branched (swallow-tail) or linear alkyl or semiperfluoroalkyl chain in lateral position have been synthesized and investigated. Besides weakly coupled lamellar isotropic ($Lam_{Iso}$), lamellar nematic ($Lam_N$) and sliding lamellar smectic phases ($Lam_{Sm}$) a sequence of three distinct types of strongly coupled (correlated) lamellar smectic phases with either centered (*c*2*mm*) or non-centered rectangular (*p*2*mm*) lattice and an intermediate oblique lattices (*p*2) were observed depending on chain length, chain branching and degree of chain fluorination. This new sequence is explained by the strengthening of the layer coupling and the competition between energetic packing constraints and the entropic contribution of either longitudinal or tangential fluctuations. This example of directed side chain engineering of small generic model compounds provides general clues for morphological design of two-dimensional and three-dimensionally coupled lamellar systems involving larger π-conjugated molecular rods and molecular or supramolecular polymers, being of actual interest in organic electronics and nanotechnology.

**Key words**: Self-assembly, liquid crystals, two-dimensional materials, soft matter, side chain engineering, perfluoroalkyl chains, columnar phases, polyphiles, π-conjugated rods

10.1002/chem.201802050

## 1. Introduction

Two-dimensional (2d) covalent molecular and self-assembled supramolecular organic materials are receiving significant interest in both academic and industrial fields due to their unique physical, chemical and mechanical properties.[1,2] The coupling of individual 2d sheets is known to lead to a transition from 2d to 3d systems which modifies their properties and determines potential applications.[3] This effect of dimensionality is especially important in soft-matter systems, such as lamellar liquid crystals (LC) composed of stacks of fluid single- or bi-molecular layers.[4,5,6] In these fluid lamellae long range order becomes unstable by layer decoupling below a critical dimensionality due to the Kosterlitz-Thouless instability.[7] This was, for example, recognized during the search for non-viral vectors for transport of DNA across membranes,[8] which initiated the study of lyotropic DNA-cationic-lipid complexes.[9,10] It was shown by Safinya et al. that the helical DNA strands are intercalated in galleries between lipid lamellae in 3d stacks of 2d layers.[9] For these systems Golubovic et al. and Lubensky et al. developed a theory and predicted different modes of DNA order depending on the strength of intralayer and interlayer coupling of the semiflexible DNA strands.[11]

Herein we report on the development of long range order depending on layer coupling at the 2d-3d transition in self-assembled lamellar LCs formed by π-conjugated molecular rods with polar groups at both ends and carrying a laterally tethered linear or branched alkyl or semiperfluoroalkyl chain (Figure 1, Chart 1).[12-17] Numerous different modes of soft self-assembly have recently been observed for these T-shaped polyphilic molecules (Figure 1). They typically form columnar LC phases where the rod-like cores build the walls of honeycombs, held together at the edges by hydrogen bonding between the polar groups and the resulting prismatic cells being filled with the flexible lateral chains (c-h).[12,13] Depending on the chain volume relative to the rod length, different polygonal cross sections were found for these honeycombs, ranging from triangular via rhombic, square, pentagonal, hexagonal (c-

10.1002/chem.201802050

f)[13] to giant hexagonal with either 8 or 10 molecules in the circumference (g,h).[15,16,17] With further increasing chain volume the honeycombs first burst open forming lamellar phases (Lam, i-l).[14] Finally, with the side-chains expanding further, the lamellae break up into ribbons, cubic networks (m,n) [18,19] and eventually hexagonal columnar phases (o), in all three latter cases comprising coaxially aligned molecular bundles.[20]

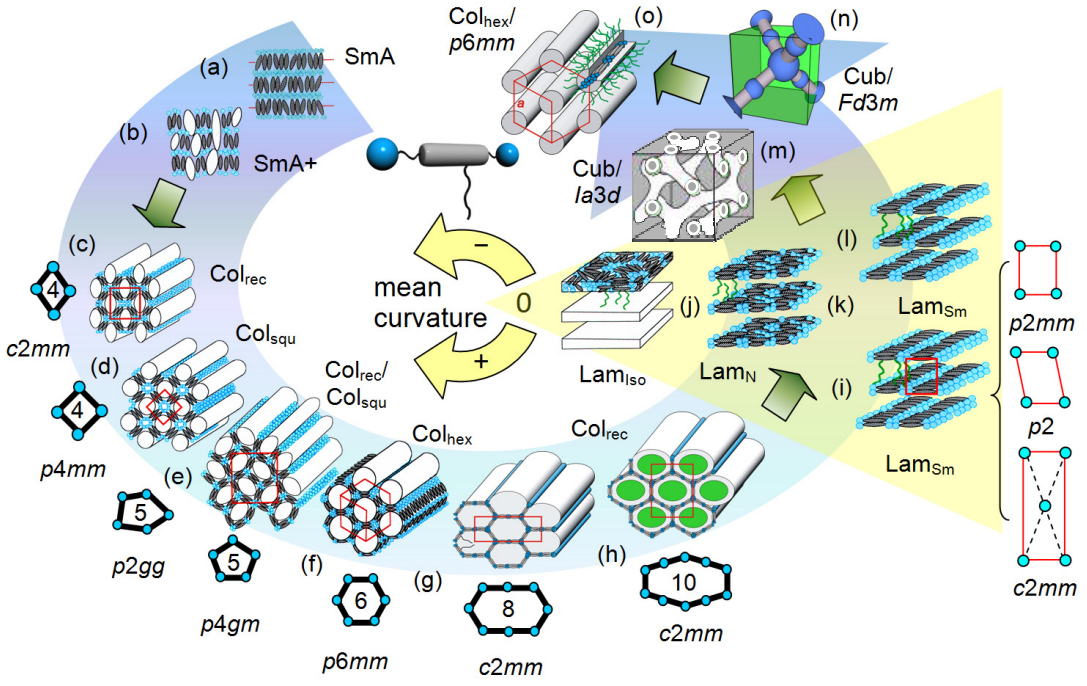


**Figure 1**. Selected self-assembly modes of T-shaped bolapolyphiles with increasing lateral chain volume (anticlockwise). Starting from conventional smectic layers (a), with increasing side-chain volume the structure evolves through modulated smectics (b), a series of columnar honeycombs with increasing number of molecules contained in cell circumference (c-h), via lamellar structures with mesogens parallel to the layers (i-l), via network cubic phases (m, n), finally ending in coaxial rod-bundle hexagonal phases (o), the inverse of the honeycombs.[12] The in-plane smectics (Lam phases) in the yellow triangle (i-l) are 90-degree tilted versions of the previously known smectic LC phases (a).

The lamellar phases (i-l) in the yellow triangle in Figure 1 are in the focus of this contribution. In these Lam phases, ranging from lamellar isotropic ($Lam_{Iso}$) via lamellar nematic ($Lam_N$) to lamellar smectic ($Lam_{Sm}$), the π-conjugated rods are either disordered ($Lam_{Iso}$) or predominantly aligned *parallel* to the layer planes and the layers of the aromatic rods are

10.1002/chem.201802050

mutually coupled/decoupled by layers of the fluid lateral chains.[14-16,21,22] All these Lam phases are different from the usual smectic LC phases (Sm phases, Figure 1a) where the rods are either perpendicular to the layer planes (SmA) or slightly tilted with respect to the layer normal (SmC).[4,5] In previous work it was shown that layering by core-chain segregation takes place in the $Lam_{Iso}$ phases (j), followed at lower temperatures by the establishment of long range orientational order between the rod-like cores at the $Lam_{Iso}$-$Lam_{N}$ transition (k), finally followed by the continuous development of positional in-plane correlation between rows of molecules in the $Lam_{Sm}$ phases (i,l).[21,22] The weakly coupled in-plane smectics are in some respect related to the above mentioned DNA-lipid complexes.

**Chart 1.** T-shaped Ternary Bolapolyphiles Under Investigation. [a]

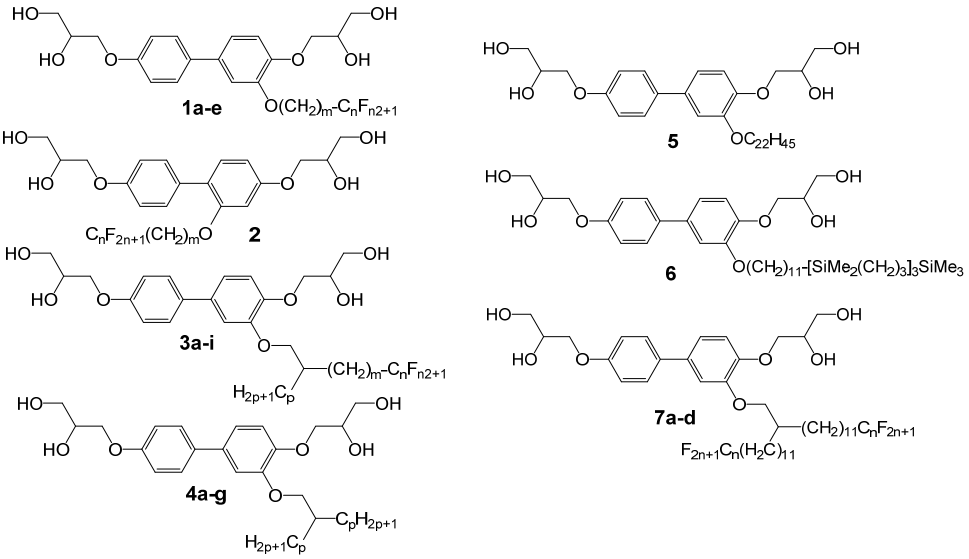


[a] Compounds **1a**, **1c-e**, **2, 3b-e**, **3g**,**h**, **4a-d** and **4f**,**g** represent newly synthesized compounds, whereas **1b**,[14b] **3a**,[17] **3f**[22] and **4e**[15] have been shortly communicated previously and **5-7**[15,16,18] represent known compounds which were included for comparison purposes (for *m, n, p*, see Tables 1-5).

In this report we focus on the development of a series of four different modes of layer coupling in the $Lam_{Sm}$ phases, three of them with 2d lattice (red parallelograms in Figure 1i, right). It is shown that the strength and mode of layer coupling can be controlled by side-chain engineering, i.e. by chain fluorination[23] and chain branching, as well as by changing

10.1002/chem.201802050

chain volume and tethering position (Chart 1). With decreasing coupling of the layers the stacking mode of the rows of molecules forming the layer changes from AB (centred rectangular, plane group *c*2*mm*), favoured in strongly coupled systems, via an intermediate oblique *p*2 lattice to AA coupling (non-centred rectangular, *p*2*mm*) and finally to the positionally non-correlated $Lam_{Sm}$ phases (designated herein as "sliding" $Lam_{Sm}$ phases) and the $Lam_{N}$ and $Lam_{Iso}$ phases for even weaker layer coupling at enhanced temperature. Thus, the generic phase sequence of the *in-plane smectics* (Lam phases), representing the 90° tilted relatives of the classical smectic LC phases, is established. Though the correlated $Lam_{Sm}$ phases with 2d lattices could alternatively be regarded as lamello-columnar phases,[24] here, we reserve the term columnar (Col) for the polygonal honeycomb structures (Figure 1c-h) and coaxial rod-bundle phases (Figure 1o).[15,17] Overall, this work provides clues for the general understanding and precise control of the self-assembly of well-defined structures built up by π-conjugated molecular rods, and as such is of interest for morphological design of organic electronics, light harvesting and other advanced materials.[6,24-27]

## 2. Results and Discussion

### 2.1 Synthesis

Scheme 1 describes the general synthetic pathway to compounds **1**-**4**. The synthetic procedures and analytical data of the compounds are reported in the SI.[28] The syntheses of compounds **5-7**, included in the discussions, have been reported previously.[15,16,18] All compounds **1-7** with exception of **4b**,**c** show enantiotropic, i.e. thermodynamically stable LC phases, only the mesophases of **4b**,**c** are monotropic, i.e. these can only be observed on cooling.

10.1002/chem.201802050

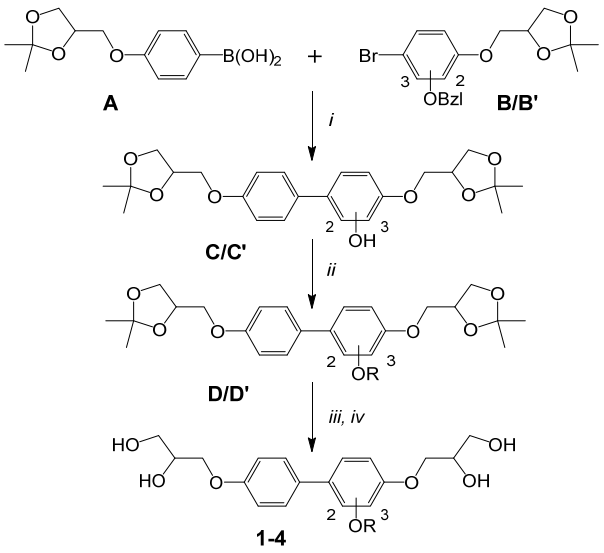


Scheme 1. Synthesis of compounds **1-4** (position and structure of R are defined in Chart 1 and Tables 1-5) from **A**[13a] and **B** (2-substituted)[15] or **B'** (3-substituted), respectively. Reagents and conditions: *i*) $Pd(PPh_3)_4$, $NaHCO_3$, glyme, $H_2O$, reflux, 6 h; [29] *ii*) $H_2$, Pd/C, EtOAc, 30 °C, 24 h.; *iii*) RX, $K_2CO_3$, DMF, $Bu_4NI$, 50-60 °C, 6 h; *iv*) 10 % HCl, MeOH, reflux, 6 h.

## 2.2 Liquid crystalline self assembly

### 2.2.1 Compounds with linear alkyl-fluoroalkyl chains - transition from sliding to weakly locked layers

The compounds of series **1** (Table 1) can be divided into two groups, the majority forming the phase sequence $Lam_{Iso}$, $Lam_N$ and $Lam_{Sm}$ (**1b**,**c**,**e**) and those showing exclusively the $Lam_{Sm}$/*p*2*mm* phase (**1a,d**). Generally, the occurrence of $Lam_N$ and $Lam_{Iso}$ phases requires longer lateral chains ($f_R \geq 0.57$) than that of $Lam_{Sm}$ phases alone. The transitions between the different subtypes of lamellar phases can be detected under the polarizing microscope as shown in Figure 2a-f.[14] In planar alignment (layers predominately perpendicular to the surfaces) the $Lam_{Sm}$ phases developing in the sequence $Lam_{Iso}$–$Lam_N$–$Lam_{Sm}$ are characterized by typical fan-like textures with increasing birefringence due to the growing in-plane order parameter (Figure 2b,d,f). However, planar alignment can only rarely be obtained, and then only over small areas. The usually observed mode of alignment is homeotropic,[21b] i.e. with the layers parallel to the surfaces, as also confirmed by XRD investigations (*vide*

10.1002/chem.201802050

*infra*). In homeotropic regions the $Lam_{Iso}$–$Lam_N$ transition is characterized by schlieren textures and, in the $Lam_{Sm}$ phase, by the formation of focal conic-like domains due to the emerging in-plane periodicity (Figure 2a,c,e).[21c] If formed directly from the isotropic liquid (compounds **1d** and **1a**), the alignment is also homeotropic and $Lam_{Sm}$ displays typical developable domain ("spherulitic") texture, reminiscent of LC phases with 2d-lattice, whether or not a 2d periodicity could be detected by X-ray diffraction (see Figures 2g,h).

**Table 1.** Mesophases of Compounds **1** and **2** with Linear Semiperfluorinated Lateral Chains.[a]

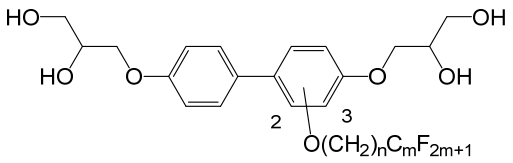


| Comp. | *Pos.* | *n* | *m* | *T* /°C<br>Δ*H* / kJ·mol$^{-1}$ | Lattice parameters<br>*d*/nm[b] | *a*/nm | *b*/nm | $f_R$ | $n_{wall}$ |
|---|---|---|---|---|---|---|---|---|---|
| **1a** | 3 | 6 | 8 | Cr 120 $Lam_{Sm}$[c] 159 Iso<br>*47.3* *5.1* | 3.7 | | | 0.52 | 3.0 |
| **1b**[14b] | 3 | 6 | 10 | Cr 135 $Lam_{Sm}$ ~165 $Lam_N$ 166 $Lam_{Iso}$ 195 Iso<br>*67.8* *2.6* *1.1* | 4.0 | | | 0.57 | 3.1 |
| **1c** | 3 | 6 | 12 | Cr 143 $Lam_{Sm}$ ~165 $Lam_N$ 169 $Lam_{Iso}$ 234 Iso<br>*69.5* *2.5* *1.8* | 4.4 | | | 0.59 | 3.1 |
| **1d** | 3 | 11 | 6 | Cr 111 $Lam_{Sm}$/*p2mm* 147 Iso<br>*34.8* *4.2* | *3.7* | 3.7 | 1.8 | 0.55 | 2.9 |
| **1e** | 3 | 11 | 8 | Cr 120 $Lam_{Sm}$ ~157 $Lam_N$ 158 $Lam_{Iso}$ 179 Iso<br>*39.6* *2.7* *0.6* | 4.2 | | | 0.58 | 3.1 |
| **2** | 2 | 6 | 10 | Cr 95 $Lam_{Sm}$ ~115 $Lam_N$ 129 $Lam_{Iso}$ 173 Iso<br>*14.0* *0.6* *0.7* | 4.0 | | | 0.57 | 3.1 |

[a] Transition temperatures and corresponding enthalpy values (lower lines in italics) were taken from the first DSC heating scans (10 K min$^{-1}$, see Figures S3-S4d); the continuous $Lam_{Sm}$-to-$Lam_N$ transitions were estimated by polarizing microscopy as the temperature at which the typical schlieren texture in the homeotropic aligned regions has disappeared; abbreviations: Cr = crystalline solid, Iso = isotropic liquid state; $Lam_{Iso}$ = lamellar isotropic phase; $Lam_N$ = lamellar nematic phase, $Lam_{Sm}$ = sliding lamellar smectic phase, $Lam_{Sm}$/*p2mm* = correlated $Lam_{Sm}$ phase with AA correlation of adjacent layers and non-centred rectangular *p2mm* lattice; $f_R$ = volume fraction of the lateral chain determined by using crystal volume increments;[30] $n_{wall}$ = average number of molecules in the cross section of the aromatic layers of the $Lam_{Sm}$ phases; for $Lam_{Sm}$ and $Lam_{Sm}$/*p2mm* it corresponds to $n_{cell}$; $n_{cell}$ = number of molecules in a unit cell defined by the dimensions $V_{cell}$ = 1.8 nm × 0.45 nm x *d* and calculated as $n_{cell} = k \times V_{cell}/V_{mol;}$ $V_{mol}$ was calculated from volume increments;[30] $k$ = 0.893 is a correction for the packing density in the LC state: $k = (V_{cryst} + V_{liqu})/2$; (for details of calculations, see Table S2 and for XRD data see Figures S6-S9 and Table S1). [b] *d* refers to the $Lam_{Sm}$ phases; [c] according to the optical textural similarity with **1d** the $Lam_{Sm}$ phase of this compound is most probably $Lam_{Sm}$/*p2mm*, too (see Figure 2g).

10.1002/chem.201802050

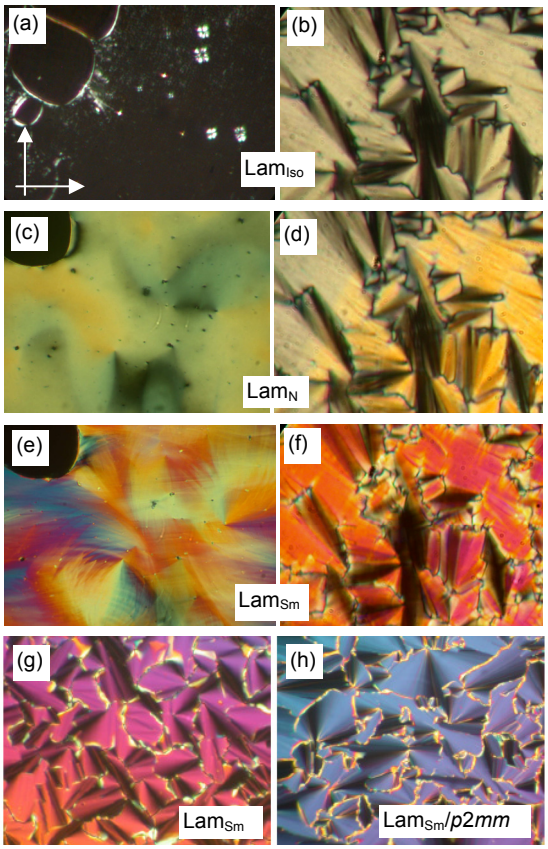


**Figure 2**. Representative textures of the different types of Lam phases formed by compounds **1** as observed between crossed polarizers. (a-f) compound **1c**: (a,b) at 200 °C, in the $Lam_{Iso}$ phase, (c,d) at 168 °C in the $Lam_{N}$ phase; (e,f) in the $Lam_{Sm}$ phase at 139 °C; the series (a→c→e) shows the development of the textures in a homeotropically aligned sample (layers parallel to the substrate, view perpendicular to the layers) whereas the series (b→d→f) shows the textural changes in regions with predominately planar alignment (layers predominantly perpendicular to the substrate), both on cooling. (g,h) Developable domain (spherulitic) textures as typically observed for the $Lam_{Sm}$ phases formed directly from the isotropic liquid: g) $Lam_{Sm}$ phase of compound **1a** without observable 2d lattice at 153 °C and h) $Lam_{Sm}$/*p2mm*-phase of compound **1d** at 140 °C.

Figure 3a-d shows the diffraction patterns of an aligned sample of **1e** in the $Lam_{Iso}$ and $Lam_{Sm}$ phases. In the small angle range only the layer reflection with its higher orders appear on the meridian, confirming that the layers are parallel to the substrate surface (X-ray beam is parallel to the substrate), as also found for the diffraction patterns of all other compounds reported herein.

10.1002/chem.201802050

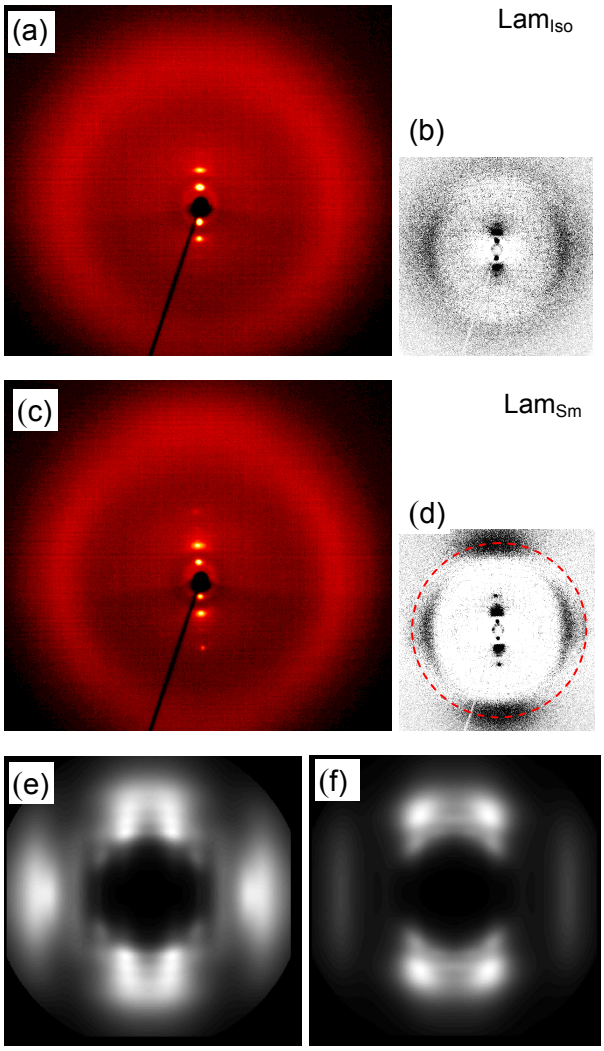


**Figure 3**. a-d) X-ray diffraction pattern of a surface aligned sample of compound **1e** (beam parallel to the substrate); (a,b) in the $Lam_{Iso}$ phase at 170 °C, and (c,d) in the $Lam_{Sm}$ phase at 110 °C; (a,c) show the original diffraction patterns and b,d) the patterns after subtraction of the patterns in the isotropic phase, $I_{rel} = I(T)–I(Iso)$; for XRD patterns of other compounds **1** and **2**, see Figures S6-S9. e,f) Simulated fiber diffraction patterns (WAXS region) of a model compound (see Figure S24), e) with the $R_F$ segments perpendicular to the layers and f) with the $R_F$ segments almost parallel to the layers respectively (fiber axis vertical).

In the original patterns (Figures 3a,c) the azimuthal distribution of WAXS intensity is almost uniform. In order to enhance the modulation in azimuthal intensity distribution, scattering from the isotropic liquid was subtracted (Figures 3b,d). In the $Lam_{Iso}$ phase (Figure 3b) there are distinct WAXS maxima at the equator, corresponding to a mean distance of 0.55 nm. These maxima, characteristic of lateral interference from perfluorinated chains, indicate that the preferred direction of the fluorinated segments is perpendicular to the layer planes.

10.1002/chem.201802050

The WAXS corresponding to a mean distance of 0.45 nm remains as a closed ring, with apparently little preferred orientation of the hydrocarbon segments (biphenyls and alkyl spacers). In contrast, in $Lam_{Sm}$ the WAXS has clear maxima near the meridian (at 0.45 nm) and the equator (at 0.55 nm, see Figure 3d). From packing estimates (see Table 1 and discussion further below) it is concluded that the aromatic layer consists of three layers of in-plane biphenyl-glycerol cores ($n_{wall}$ ~3). Optimized space filling requires that the alkyl spacers are nearly parallel to the layer plane (Figure S25b). Thus, the meridional maximum at 0.45 nm is attributed to scattering of the multiple layers of hydrocarbon moieties, aromatic and aliphatic, with a total thickness of ca. ~2 nm. This value corresponds roughly to the correlation length extracted from the radial width of the WAXS. To check how the organization of the different molecular segments could influence the WAXS patterns, the patterns from two alternative structural models of the $Lam_{Sm}$ phase were simulated for a model compound with (a) tilted but not interdigitated and (b) perpendicular and interdigitated $R_F$ chains (Figure S24b,d). The results, displayed in Figure 3e,f, respectively, show that significant meridional scattering could be observed for both models. However, strong equatorial scattering is only observed for the model with the fluorinated chains normal to the layer plane (Figure 3e). Hence, it can be concluded that despite the relatively high degree of disorder (nearly isotropic distribution of WAXS in the original patterns), in all LC phases of compounds **1** there is some preference of the $R_F$ chains to align normal to the layers.

Figure 4a shows the change in layer spacing and diffraction intensity on heating the methyl branched compound **3a** (see Table 3) from the $Lam_{Sm}$ via $Lam_N$ to the $Lam_{Iso}$ phase. Generally, the layer spacing of the Lam phases does not vary greatly with temperature; over the entire Lam range the layer *d*-spacing remains within 0.1 nm.

10.1002/chem.201802050

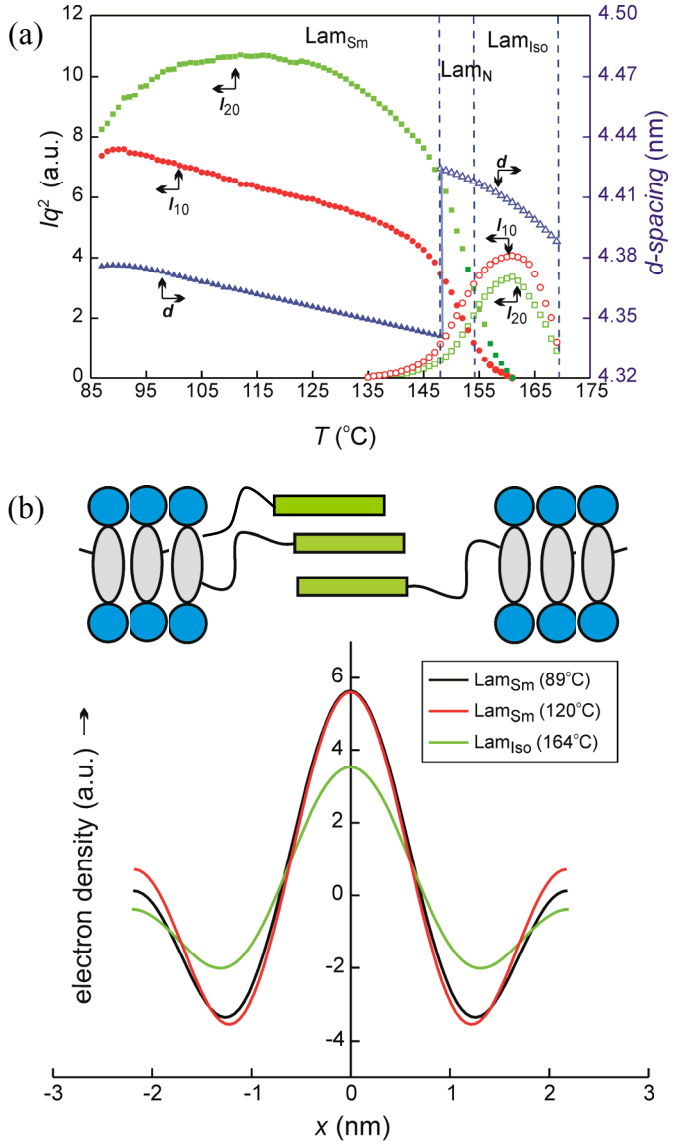


**Figure 4**. a) Layer spacing (blue) and intensities of the two strongest layer reflections (red, green) in the $Lam_{Sm}$ phase (full symbols) and the $Lam_N$/$Lam_{Iso}$ phases (empty symbols) recorded for the methyl-substituted compound **3a** (Table 3); b) electron density profiles normal to the layer, reconstructed from SAXS intensities at the temperatures indicated. The large and the small maxima correspond, respectively, to the fluorinated and aromatic sublayers, as indicated by the schematic model of a layer in (b). The densities are on an arbitrary but internally consistent scale (for details of the method see SI, for electron density maps of the $Lam_{Sm}$ phase of **1b**, see Figure S23a,b).

The electron density profiles in Figure 4b (for compound **1b**, see Figure S23a,b) indicate a triply segregated layer structure with high electron density assigned to the layers of the $R_F$ chains which are separated from the aromatic layers (medium density) by layers formed by

10.1002/chem.201802050

the aliphatic spacers (lowest electron density). The lower local maxima, assigned to the aromatic layers, show a small increase in height on heating the $Lam_{Sm}$ phase from 85 °C to ca. 120 °C. This is likely to be the result of some layer perfection at higher temperatures. However, with further temperature increase both the $R_F$ and the aromatic maxima decrease again, indicating that in the $Lam_N$ and especially in the $Lam_{Iso}$ phase the boundaries between the sublayers become more diffuse, and that in the aromatic layers there is a substantial drop in the smectic order parameter,[31] which is in line with all other data.

With decreasing temperature the growing strength of layer coupling is expected to give rise to the development of positional order within and presumably also between the aromatic layers. However, only for the $Lam_{Sm}$ phase of compound **1d** additional weak X-ray reflections become visible on zeroth and first layer lines after long exposure (see Figure S8a). This compound has the shortest $R_F$ end group ($C_6F_{13}$), its $Lam_{Sm}$ phase has the smallest layer *d*-spacing and is formed directly from the isotropic liquid without the intervening $Lam_{Iso}$ and $Lam_N$ phases. The diffraction pattern can be indexed on a simple rectangular lattice (*p2mm*) with parameters $a$ = 3.7 nm and $b$ = 1.8 nm ($Lam_{Sm}$/*p2mm* phase). As the length of the bolaamphiphilic core is between 1.7 nm and 2.1 nm, depending on the conformation of the glycerol groups, $b$ is assigned to correspond to the effective length of the core in the layers and $a$ to the layer spacing. Parameter $a$ fits well with the periods $d$ observed for the other members of series **1** (see Table 1). This non-centered *p2mm* lattice implies AA stacking of the rows of molecules in the layer (Figure 1i). In actual fact it is likely that the $Lam_{Sm}$ phase of **1a** with $d$ = 3.7 nm, also lacking the $Lam_{Iso}$ and $Lam_N$ phases, has correlated layers, too, albeit with a shorter correlation length. While 0*k* or *hk* reflections were not seen, the texture of this compound is almost identical to that of the $Lam_{Sm}$/*p2mm* phase of **1d** (Figure 2g,h). Notably, off-meridional reflections have never been observed for any of the $Lam_{Sm}$ phases occurring below $Lam_{Iso}$/$Lam_N$, even after very long exposure (see Figure S7c), suggesting that these represent sliding $Lam_{Sm}$ phases without long range positional layer correlation.

10.1002/chem.201802050

To improve our understanding of the phase structure we need to estimate the number of molecules per unit area of the layer or, in other words, the thickness of the walls separating the layers of the lateral chains. We base our calculation on the volume of a molecule $V_{mol}$, and the volume of a hypothetical 3d unit cell, $V_{cell}$, defined by the layer distance $d$, the bolaamphiphilic core length (1.8 nm), and an assumed lateral molecular separation of 0.45 nm (Tables 1 and S2). The 0.45 nm separation is commonly found in these mesogens and is supported also by the position of the meridional WAXS maximum. The number of overlying molecules in the aromatic (biphenyl + glycerol) layer, $n_{wall}$, is then equal to the number of molecules in such a cell, $n_{cell}$. For compounds **1** and **2** $n_{wall}$ is calculated as close to three (see Tables 1 and S2). Double molecule walls, containing an arrangement of only two biphenyl cores back-to-back ($n_{wall} \sim 2$) would allow all side-chains easy access to the alkyl-fluoroalkyl sublayer and thus should be preferred. However, the fact that thicker three molecule walls form, where some packing frustration arises for the chains of the molecules in the middle, might be due to a combination of different effects. In general, increasing $n_{wall}$ reduces the aromatic aliphatic interfacial area per volume unit and also allows formation of hydrogen bonding networks (see IR data in Figure S5 and associated explanations) with increased diameter, providing more and stronger hydrogen bonding which contribute to stabilization of triple layers, and compensating the developing packing frustration due to the inevitable core-chain interaction. In addition, most compounds have their alkyl chains at the periphery of the biphenyl core, next to one of the glycerols, and therefore their distorting effect on the packing of these cores is relatively small (see Figure S25b). Only the steric distortion provided by a lateral chain in the central 2-position (compound **2**) is larger, thus leading to the observed expansion of the $Lam_{Iso}$ and $Lam_N$ ranges and stronger destabilization of $Lam_{Sm}$ (Table 1). An additional triple layer stabilizing effect, related specifically with the partly fluorinated chains of compounds **1** and **2**, might arise from the fact that the interfacial area of a biphenyl core (1.8 nm x 0.45 nm = 0.81 $nm^2$) is about 1.5 times that of the area required by a pair of

interdigitated $R_F$ chains (0.54-0.62 nm$^2$). In order to retain flat interfaces one additional $R_F$ chain is required which is provided by the third molecule. Interestingly, there appears to be a relation between the measured layer distance *d* and the observed phase sequence. All compounds of series **1** with $d \geq 4.0$ nm form the phase sequence $Lam_{Iso}$-$Lam_N$-$Lam_{Sm}$, whereas the two compounds **1a** and **1d** with shorter distances ($d$ = 3.7 nm) show only the $Lam_{Sm}$ phase, presumably with *p*2*mm* lattice in both cases (Table 1). This is a first hint of the importance of the lamellar distance for layer coupling and thus for the observed type of Lam phase.

**Table 2.** Mesophases of Compounds **5** and **6** (see Chart 1). [15,16]

| Comp. | *T* /°C<br>$\Delta H$ / kJ·mol$^{-1}$ | *d*/nm | $f_R$ | $n_{wall}$ |
|---|---|---|---|---|
| **5** | Cr 93 $Col_{rec}$/c2*mm* [a] 117 $Lam_{Sm}$ 123 Iso<br>*7.0* *1.0* *4.4* | 3.6 [b] | 0.57 | 2.7[b] |
| **6** | Cr 117 $Lam_N$ 144 Iso<br>*38.4* *6.1* | 4.5 | 0.68 | 3.1 |

[a] The $Col_{rec}$/*c*2*mm* phase is a polygonal honeycomb phase formed by extended hexagonal prismatic cells (8-hexagons, see Figure 1g); [b] data of the $Lam_{Sm}$ phase.

T-shaped molecules with non-fluorinated linear alkyl chains ($n$ = 6-22) have been studied previously (Chart 1 and Table 2).[15] Due to the significantly smaller volume of the non-fluorinated *n*-alkyl chains compared to the fluorinated ones, compound **5** with $n$ = 22 is the first homologue in this series capable of forming a Lam phase.[15] Only the $Lam_{Sm}$ phase without accompanying $Lam_N$ and $Lam_{Iso}$ phases is observed, in line with the small layer distance $d$ = 3.6 nm, providing a strong layer coupling. Replacing the fluorinated segments at the end of the $(CH_2)_{11}$ spacers of compounds **1d**,**e** by bulkier carbosilane units (e.g. compound **6**, Chart 1)[16,15] leads to $d$ > 4.0 nm; this removes the $Lam_{Sm}$ phase completely, and instead only the $Lam_N$ phase is found over a relatively broad temperature range (Table 2). That $n_{wall}$ is close to three in all these cases suggests that the formation of triple molecule layers ($n_{wall}$ ~3)

10.1002/chem.201802050

is a general feature for linear and end-branched chains and is not specific to chains with fluorinated end-groups.

### 2.2.2 Compounds with branched and swallow-tail chains involving fluoroalkyl segments – from sliding to strongly locked layers

Compound **3a** having a methyl branched semiperfluorinated chain shows the same phase sequence involving $Lam_{Iso}$, $Lam_N$ and $Lam_{Sm}$ phases (Table 3, Figure 4) as observed for most non-branched compounds **1** (Table 1). The methyl group in the chain of **3a** appears to be small enough to retain the triple layer structure ($n_{wall}$ = 2.9), albeit causing a shift to lower temperatures ($\Delta T \leq 10$ K), presumably due to some steric distortion by the additional methyl groups.

In contrast, compound **3b** (Table 3, Figures 5a,b and S10), having an only slightly longer *n*-propyl branch, behaves very differently; it only forms $Lam_{Sm}$/*p*2*mm*, indicating stronger layer coupling in spite of having a chain volume larger than **1e**. The layer distance $d = a$ = 3.9 nm is also reduced compared to the *d*-values of the Lam phases of related compounds **1e** with linear chains ($d$ = 4.2 nm) and the methyl substituted compound **3b** ($d$ = 4.3 nm). The synchrotron GISAXS pattern indicates the presence of very weak additional off-meridional (01) and (11) reflections of a *p*2*mm* lattice (Figure S10). That these spots are sharp indicates long-range layer correlation albeit with very weak in-plane electron density modulation, presumably partially because of the small electron density difference between biphenyls and glycerols. That positional order is induced between **3a** to **3b** is the first indication that chain branching close to the core disfavors triple layer formation (reduction of $n_{wall}$ to 2.5) and thus reduces the layer distance.

10.1002/chem.201802050

**Table 3.** Mesophases of Compounds **3** with a Branched Semiperfluorinated Lateral Chain. [a]

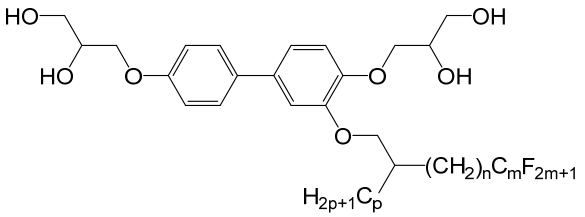


| Comp. | *m* | *n* | *p* | *T* /°C<br>Δ*H* /kJ·mol$^{-1}$ | Lattice parameters /nm | | | $f_R$ | $n_{wall}$ |
|---|---|---|---|---|---|---|---|---|---|
| | | | | | *d* | *a* | *b* | | |
| **3a**[17] | 8 | 11 | 1 | Cr 60 $Col_{rec}$/*c*2*mm* 89 $Lam_{Sm}$ ~149 $Lam_N$ 155 $Lam_{Iso}$ 169 Iso<br>*12.1* *0.3* *3.2* *0.8* | 4.3[b] | | | 0.61 | 2.9 |
| **3b** | 8 | 11 | 3 | Cr 54 M1 85 $Lam_{Sm}$/*p*2*mm* 150 Iso<br>*2.9* *0.5* *6.7* | *3.9* | 3.9 | 1.8 | 0.63 | 2.5 |
| **3c** | 4 | 3 | 7 | Cr 73 $Lam_{Sm}$/*c*2*mm* 126 Iso<br>*24.7* *8.0* | *2.6*[c] | 5.2 | 1.8 | 0.52 | 2.2[d] |
| **3d** | 6 | 3 | 7 | Cr 64 $Lam_{Sm}$/*p*2*mm* 134 Iso<br>*20.8* *7.9* | *2.8* | 2.8 | 1.9 | 0.56 | 2.1 |
| **3e** | 8 | 3 | 7 | Cr 61 $Lam_{Sm}$/*p*2*mm* 144 Iso<br>*19.1* *8.2* | *3.1* | 3.1 | 1.8 | 0.59 | 2.2 |
| **3f**[22] | 6 | 3 | 9 | Cr 66 $Lam_{Sm}$/*p*2*mm* 131 Iso<br>*21.6* *7.3* | *2.7* | 2.7 | 1.7 | 0.58 | 2.0 |
| **3g** | 4 | 3 | 11 | Cr 51 $Lam_{Sm}$[c] 111 Iso<br>*14.0* *4.5* | 2.7 | | | 0.57 | 2.0 |
| **3h** | 6 | 3 | 11 | Cr 61 $Lam_{Sm}$/*p*2*mm* 124 Iso<br>*20.3* *6.8* | *2.9* | 2.9 | 1.8 | 0.60 | 2.0 |
| **3i** | 8 | 3 | 11 | Cr 57 $Lam_{Sm}$/*p*2*mm* 132 Iso<br>*15.6* *6.4* | *3.2* | 3.2 | 1.8 | 0.63 | 2.1 |

[a] for conditions and abbreviations, see Table 1; additional abbreviations: $Lam_{Sm}$/*c*2*mm* = rectangular columnar phase with *c*2*mm* lattice ($Lam_{Sm}$ phase with AB correlation of adjacent layers); $Col_{rec}$/*c*2*mm* phase = polygonal honeycomb phase formed by extended hexagonal prismatic cells (8-hexagons, see Figure 1g); for XRD data, see Figures S10-S15 and Tables S1 and S2; [b] *d* refers to the $Lam_{Sm}$ phase; [c] according to the textural similarity with the other compounds **3b-f** it is most probably $Lam_{Sm}$/*p*2*mm*, too (see Figure S1a); [c] $d = a/2$; [d] $n_{wall}$ of the $Lam_{Sm}$/*c*2*mm* phase is obtained by dividing $n_{cell}$ by 2 (for details of the calculations, see Tables 1 and S2).

Even more strongly reduced *d*-values (*d* = 2.4-3.2 nm) were found for all compounds **3c-i** (Table 3) with lateral chains having two equally long branches and the branching point positioned close to the aromatic core (so-called "swallow-tailed" compounds). All of them form exclusively the $Lam_{Sm}$ phase, irrespective of chain length, chain volume and the degree of fluorination. The textures of all these $Lam_{Sm}$ phases, formed directly from the isotropic liquid state, are almost identical, characterized by dendritic growth of X-shaped or rectangular

10.1002/chem.201802050

domains which coalesce to mosaic-like textures (Figures 5c-f), indicating relatively rigid layers.

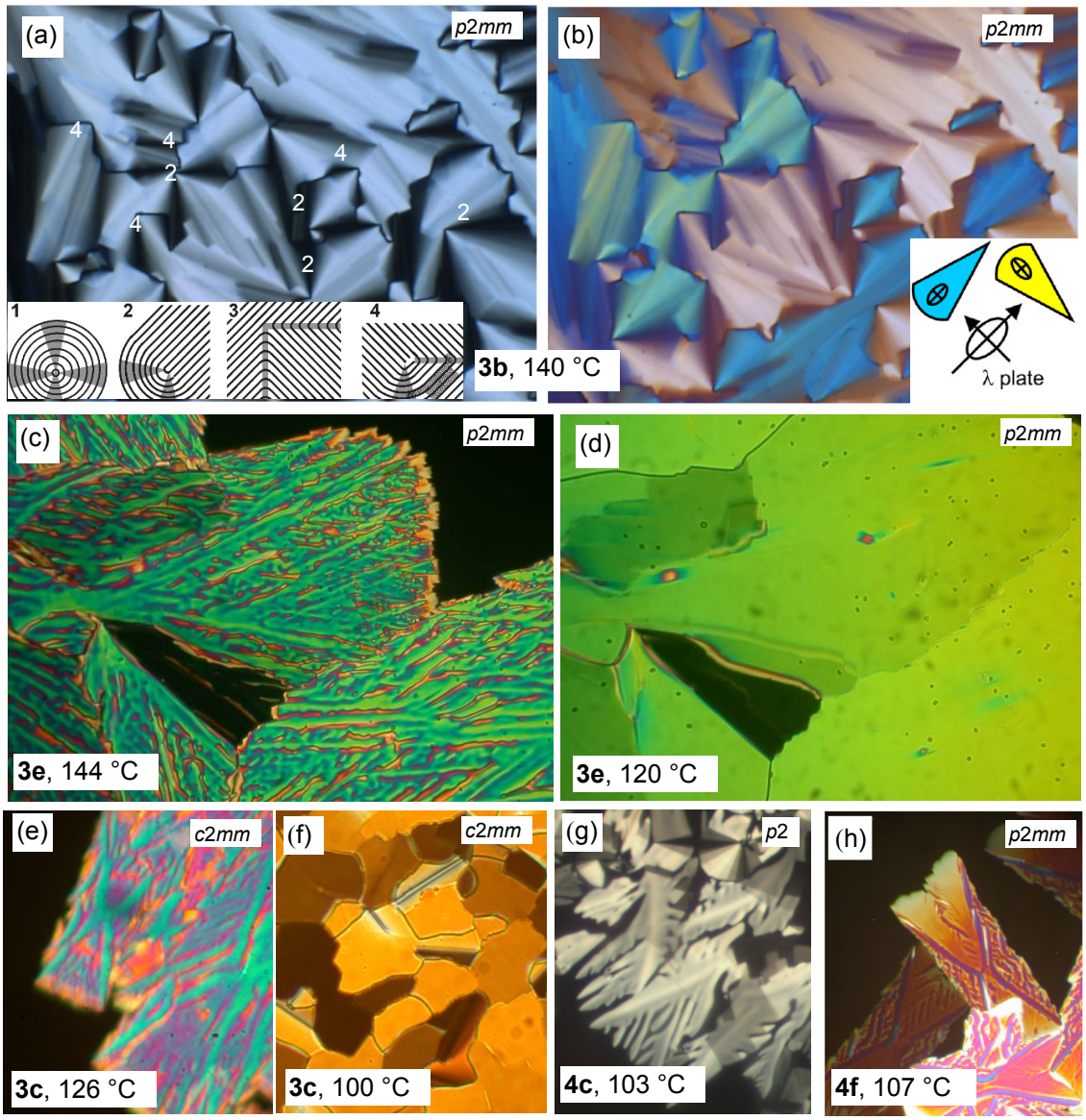


**Figure 5.** Selected textures of correlated $Lam_{Sm}$ phases as observed for compounds **3** and **4** between crossed polarizers: a) Texture of the $Lam_{Sm}$/*p2mm* phase of **3b** at 140 °C, b) same area with additional λ retarder plate: The indicatrix orientation is shown in the inset; the alignment of the layers is homeotropic, i.e. with the layers parallel to the substrate surface; the inset shows four potential types of defects, two of which are seen and in some cases labeled in the micrograph; the parallel lines are in the direction of *a*-axis separated by *b*, the molecular core length; the inset in (b) shows the orientation of the indicatrix, i.e. the molecular cores, in the blue and yellow areas, accordingly, these 90-degree smectics are negatively birefringent. c) Dendritic growths of the $Lam_{Sm}$/*p2mm*-phase of compound **3e** at 144 °C (dark area at top right represents residual isotropic liquid); green areas are homeotropic (layers parallel to surface), while yellow stripes represent stacks of layers inclined to the surface, probably

10.1002/chem.201802050

perpendicular, viewed edge-on ("planar" orientation); remarkably, the shape of the growing domains reflects the lattice parameters. For example, the ratio of the long and short axes of the rectangular domains of compound **4f** in (h) corresponds closely to the lattice parameter ratio *a/b*, and the calculated angle of the cell diagonal = arctan (1.8/2.7) = 33° (see Table 4) corresponds almost exactly to the measured half-angle of 34° between the domain diagonals seen in (h). Upon further growth and fusion of the domains, the edge-on orientation is removed and completely replaced by the homeotropic texture composed of uniformly colored mosaics; d) shows the fully healed homeotropic mosaic texture of **3e** at 120 °C, with the edge-on defects annealed out. e-h) Textures of the distinct types of correlated $Lam_{Sm}$ phases of compounds **3c**, **4c** and **4f** at the indicated temperatures (dark areas in (c,e,g,h) represent residual areas of the isotropic liquid phase). Formation of fan textures in (a,b) indicates soft layers whereas the mosaics in (c-h) indicates relatively rigid layers. For additional textures, see Figures S1 and S2.

X-ray scattering experiments on surface aligned samples confirm mesophases with homeotropic alignment (layers parallel to the surfaces) and 2d lattices for all swallow tailed compounds **3b-i** (see Figure 6a,c) with the exception of compound **3g**, for which only one meridional layer reflection was observed (see Figure S14). The majority of compounds **3b-i** adopt the primitive *p*2*mm* lattice (see Figure 6c). The parameter *b,* corresponding to the length of the bolaamphiphilic core, is around 1.8 nm for all *p*2*mm* phases and the parameter *a* increases with increasing lateral chain volume from *a* = 2.7-2.8 nm (**3d,g**) to 3.2 nm (**3i**). The number of molecules per unit cell is $n_{cell}$ = 2.0 - 2.2 (see Tables 3 and S2) i.e. in the $Lam_{Sm}$ phases of all swallow tailed compounds **3c-i** the aromatic layers contain only two side-by-side lying biphenyls in thickness. This is in contrast to the Lam phases of compounds **1**, **2, 3a, 5** and **6** with linear or end- and methyl-branched side-chains that have aromatic layers three molecules thick. Formation of triple layers is inhibited here by the branching of these chains close to the aromatic cores, making the incorporation of parts of these chains into the biphenyl-glycerol layers impossible. The resulting double-molecule layers in the Lam phases of compounds **3c-i** allow all bulky swallow-tail substituents to become completely excluded

10.1002/chem.201802050

from the core layers. This leads to increased rod order and simultaneously to strongly reduced layer distances (compare Tables 1 and 3), because reduction of the number of side-by-side lying molecules in the biphenyl-glycerol walls is inevitably associated with a reduction of the chain volume in the layers between the walls by the same ratio of about one third. The reduced distance provides a much stronger coupling of the layers in the Lam phases of these swallow tailed compounds.

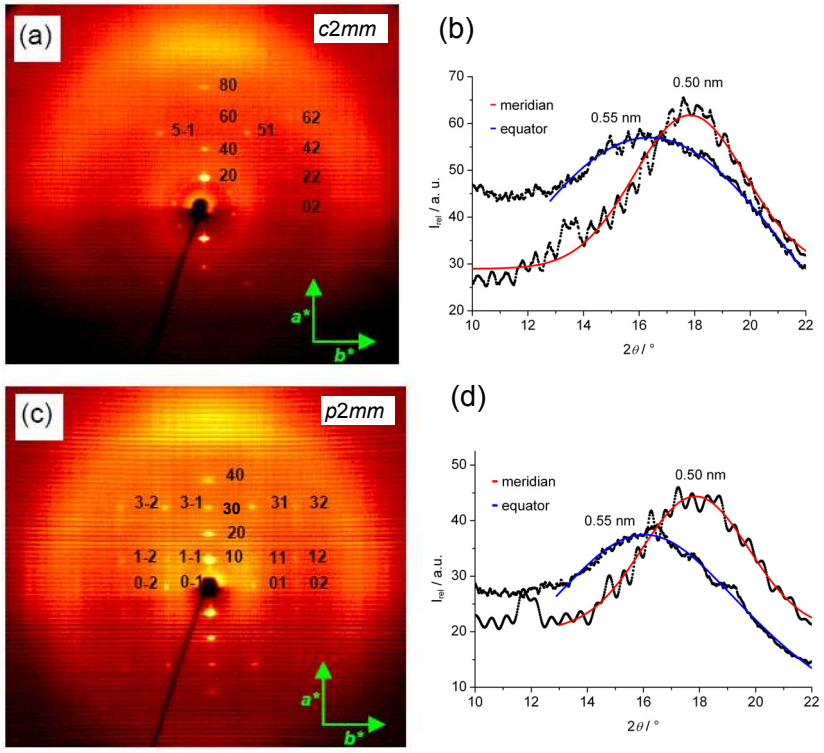


**Figure 6**. X-ray diffraction patterns of the $Lam_{Sm}$ phases. (a,b) $Lam_{Sm}$/*c2mm*-phase of compound **3c** at $T$ = 100 °C and (c,d) $Lam_{Sm}$/*p2mm*-phase of compound **3h** at $T$ = 101 °C; (a,c) original diffraction patterns (surface alignment on a glass surface, X-ray beam parallel to the surface); (b,d) $\theta$–scans of the wide angle region at $2\theta$ = 10°–22° along the meridian (red line) and along the equator (blue line; fitted Lorentzian curves).

The X-ray $\theta$-scans of the $Lam_{Sm}$/*p2mm* phase of compound **3h** are shown in Figure 6d. In contrast to the diffraction patterns of compounds **1** and **2**, distinct diffuse meridional WAXS maxima at $d$ = 0.50 nm can be observed in all diffraction patterns and these are clearly visible already in the original diffraction patterns, i.e. before background subtraction. It suggests preferred alignment of the aromatics and *all-trans*-segments of the fluid alkyl chains and also

10.1002/chem.201802050

some $R_F$ chain segments parallel to the layers. Beside these strong meridional maxima, there are weaker and azimuthally broad maxima at $d$ = 0.55 nm, centered on the equator, corresponding to the mean distance between the perfluorinated segments. The wide azimuthal distribution of this WAXS intensity suggests a random or uniform tilt of the fluorinated segments relative to the layer normal. This observation is consistent with the arrangement of the molecules as shown in the molecular dynamics annealed model in Figure 7b. Here the alkyl branches are oriented parallel to the biphenyl cores in aliphatic sublayers and the fluorinated segments are tilted and intercalated, filling the space in between. Because for the double molecule layers of the swallow tailed molecules there is no way to include an additional $R_F$ chain, tilt remains the only possible way for adjusting the cross sectional area of only two interdigitated $R_F$ chains (0.54-0.62 $nm^2$) to match that of the biphenyl-glycerol cores (0.81 $nm^2$). All these effects, reduction of $n_{wall}$, reduction of the effective chain length by branching, parallel alignment of rods and aliphatic chains and tilt of the $R_F$ segments, contribute to a reduction of $d$ and to the strengthening of layer coupling, thus leading to development of 2d layer correlation in the $Lam_{Sm}$ phases of the swallow tailed compound **3c-i**. Figure 7a shows the reconstructed electron density map of the $Lam_{Sm}/p2mm$ phase of compound **3i**. The map shows modulation reflecting the long-range in-plane and cross-layer correlation, being consistent with the proposed AA-correlated layer structure of the $Lam_{Sm}/p2mm$ phases.

Surprisingly, in contrast to all other compounds **3d-i**, for compound **3c** with the shortest swallow tailed lateral chain (and smallest layer distance, $d$ = 2.6 nm) the 2d X-ray diffraction pattern of an aligned sample (see Figure 6a,b) can be indexed to a centered rectangular lattice ($c2mm$) instead of the usually observed $p2mm$ lattice. Also for this $Lam_{Sm}/c2mm$ phase, the parameter $b$ corresponds to the length of the bolaamphiphilic core ($b$ = 1.8 nm) whereas the parameter $a$ = 5.2 nm amounts to twice the layer distance ($d$ = 2.6 nm). These parameters are

10.1002/chem.201802050

in line with a correlated layer structure with an AB sequence of adjacent layers, where a unit cell contains 4 molecules.

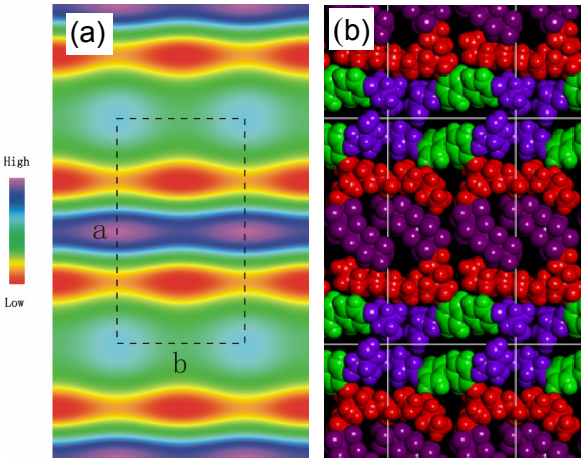


**Figure 7**. (a) Reconstructed electron density (ED) map of the $Lam_{Sm}$/*p*2*mm* phase of compound **3i** at $T$ = 70 °C (Figure S15a; for ED maps of the $Lam_{Sm}$/*p*2*mm* phase of **3b**, see Figure S23c,d); (b) snapshot of MD simulation (green = biphenyl and glycerol, purple = $R_F$, red = aliphatic); only one unit cell was used as the simulation box with periodic boundary conditions, hence the apparent translational order.

### 2.2.3 Swallow tailed compounds with two n-alkyl branches – *c*2*mm* - *p*2 - *p*2*mm* sequence

As many as three different types of $Lam_{Sm}$ phases were observed in the series of compounds **4** with branched non-fluorinated alkyl chains (Table 4). The textures of these $Lam_{Sm}$ phases (Figure 5g,h) are mosaic-like, similar to each other and almost identical to those observed for compounds **3c-i** (see Figure 5c-f). In the X-ray diffraction patterns of these compounds the diffuse wide angle scattering ($d$ = 0.45 nm) has a distinct maximum on the meridian, which is in line with a preferred organization of the biphenyls and *all-trans* segments of the fluid branched alkyl chains parallel to the layer planes (see Figure 8a).

10.1002/chem.201802050

**Table 4.** Mesophases of Swallow Tailed Compounds **4** with Two Alkyl Branches.[a]

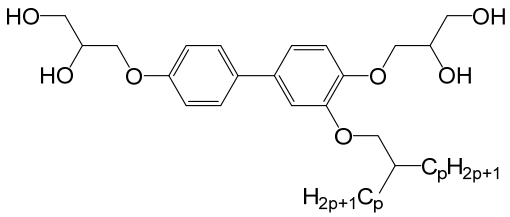


| Comp. | *p* | *T* [°C]<br>$\Delta H$ [kJ·mol$^{-1}$] | Lattice parameters/nm<br>*d* | *a* | *b* | *γ*/° | $f_R$ | $n_{wall}$ |
|---|---|---|---|---|---|---|---|---|
| **4a** | 6 | Cr 90 $Lam_{Sm}$/*c*2*mm* 95 Iso<br>*27.7* *4.9* | *2.4* | 4.7 | 1.8 | | 0.46 | 2.0 |
| **4b** | 7 | Cr 111 ($Lam_{Sm}$/*c*2*mm* 102) Iso<br>*38.0* *6.3* | *2.5* | 4.9 | 1.8 | | 0.49 | 2.1 |
| **4c** | 8 | Cr 107 ($Lam_{Sm}$/*p*2 103) Iso<br>*36.0* *6.1* | *2.6* | 2.6 | 1.8 | 102 | 0.52 | 2.2 |
| **4d** | 9 | Cr 69 $Lam_{Sm}$/*p*2*mm* 101 Iso<br>*20.3* *4.3* | *2.6* | 2.6 | 1.8 | | 0.55 | 2.1 |
| **4e**[15] | 10 | Cr 70 $Lam_{Sm}$[b] 105 Iso<br>*20.3* *5.7* | 2.7 | | | | 0.57 | 2.1 |
| **4f** | 11 | Cr 81 $Lam_{Sm}$/*p*2*mm* 107 Iso<br>*10.9* *6.6* | *2.7* | 2.7 | 1.8 | | 0.59 | 2.0 |
| **4g** | 14 | Cr 62 $Lam_{Sm}$[b] 100 Iso<br>*20.8* *6.3* | 3.1 | | | | 0.64 | 2.0 |

[a] for conditions and abbreviations, see Tables 1 and 3; values in round brackets refer to monotropic phases; $Lam_{Sm\text{-}obl}$/*p2* = correlated $Lam_{Sm}$ phase with oblique lattice; for XRD data, see Figures S16-S22 and Tables S1 and S2. [b] based on the textural similarity with compounds **4d** and **4f** it is most probably $Lam_{Sm}$/*p*2*mm* (see Figure S1b-d).

The SAXS patterns of most compounds **4** can be indexed to a 2d lattice (Figures 8a and S16-S22). This shows that layer correlation does not require fluorinated chains and hence, the segregation of alkyl and perfluorinated chains in the nonpolar layers should not be the origin of layer correlation as originally proposed in a previous communication for the $Lam_{Sm}$ phase of **3f**.[22] Instead, the occurrence of layer correlation and 2d periodicity should be a consequence of the stronger coupling of the layers of compounds with swallow tailed chains due to reduced layer distance and the parallel alignment of a significant portion of *all-trans* chain segments and aromatic cores, the latter supporting the orientational correlation of the layers.

Compounds **4a** and **4b** with the shortest chains, similarly to compound **3c**, have a *c*2*mm* lattice (AB layer correlation) with the parameters $a$ = 4.7, $b$ = 1.8 nm and $a$ = 4.9 and $b$ = 1.8 nm, respectively (Figures S16, S17). Compound **4c** with only one additional $CH_2$ group in

10.1002/chem.201802050

each of the arms shows an oblique lattice, plane group *p*2, with the parameters $a$ = 2.6 nm, $b$ = 1.8 nm and $\gamma$ = 102° (see Figure 8c,d). This lattice implies a correlated layer structure, where adjacent layers are shifted by less than ½ of the in-plane periodicity $b$, so that the *c*2*mm* plane group symmetry is lost (see Figure 9). This $Lam_{Sm}$/*p*2 phase can be regarded as an intermediate structure at the transition from *c*2*mm* to *p*2*mm*. Hence, a unique sequence of three different types of correlated $Lam_{Sm}$ phases ($Lam_{Sm}$/*c*2*mm* - $Lam_{Sm}$/*p*2 – $Lam_{Sm}$/*p*2*mm*) is observed with increasing length of the branched lateral chains.

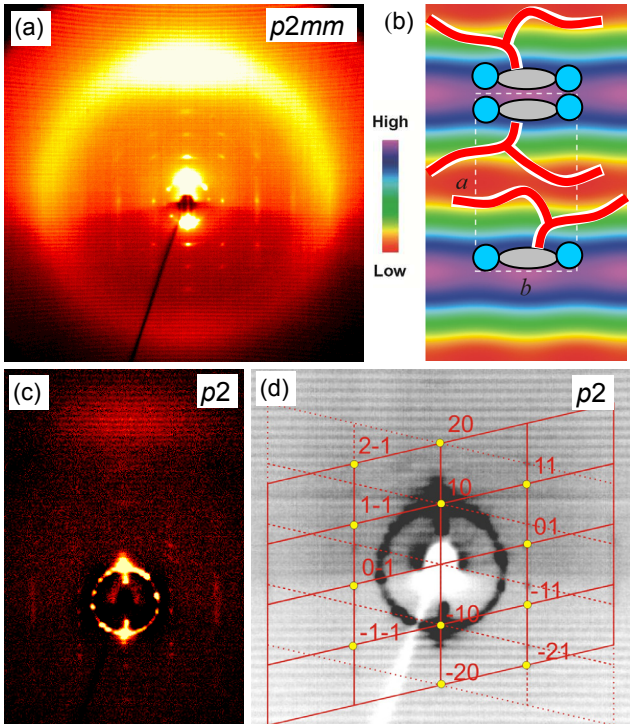


**Figure 8.** Representative XRD patterns of compounds **4.** a) X-ray diffraction pattern of a surface aligned sample of the $Col_{rec}$/*p*2*mm* phase of **4f** at 82 °C (the 4 extra spots at low angle are the strong 10 reflections from domains with different alignment, see Figure S21) and b) ED map of the $Col_{rec}$/*p*2*mm* phase of **4d** (for diffraction pattern, see Figure S19); c,d) XRD pattern of a surface aligned sample of the $Col_{rec}$/*p*2 phase of **4c** at 95 °C, c) pattern after subtraction of the Iso phase (for original pattern, see Figure S18) and d) small angle range with indexation.

The formation of a centered rectangular lattice (*c*2*mm*) with a shift by $b$/2 should be driven by optimization of space filling in the aliphatic layers, i.e. the lateral chains fill gaps in less

10.1002/chem.201802050

crowded areas (steric repulsion). Interestingly, in both series **3** and **4** the *c*2*mm* lattice is found up to a chain length of 7 carbons in each branch (Tables 3 and 4), meaning that the layer distance reaches a critical value for the *c*2*mm*-*p*2*mm* transition ($d$ = 2.6 nm, see Figures 9,10).

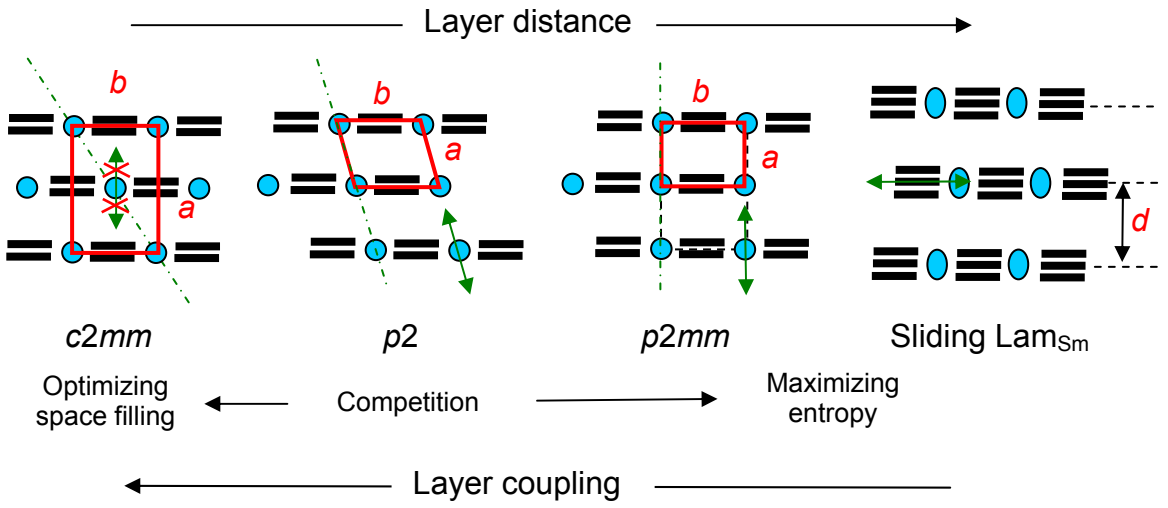


**Figure 9.** Structure variants of the Lam$_{Sm}$ organization depending on the correlation between adjacent layers, as found for the series of compounds **1**-**4**; 2d unit cells are indicated by red parallelograms, the broken lines indicate the correlation between the layers; the green arrows indicate the direction of fluctuations.

The simple rectangular lattice (*p*2*mm*) might be stabilized by attractive interaction either between the hydrogen bonding columns or between the aromatics in adjacent layers, which however appears to be unlikely as the *p*2*mm* lattice occurs upon chain elongation and thus upon layer decoupling. Therefore, it is more likely to be favored for entropic reasons, as the AA correlation enables collective out-of-plane fluctuations of the polar columns and zig-zag deformation of the layers as indicated by the green arrows in Figure 9. These tangential fluctuations become suppressed in the centered *c*2*mm* lattice. At the transition between these two packing modes the *p*2 lattice is formed as a compromise between the competing steric (enthalpic) and entropic effects. From the data in Tables 1-4 threshold *d*-values for the phase transitions of the biphenyl based bolapolyphiles can be estimated. As shown in Figure 10 these values are $d$ > 3.95 nm for sliding Lam$_{Sm}$ and Lam$_{N}$/Lam$_{Iso}$ phases, and $d$ < 3.95 nm for

the correlated $Lam_{Sm}$ phases with $2.6 > d < 3.95$ nm for $Lam_{Sm}/p2mm$, $d \sim 2.6$ nm for $Lam_{Sm}/p2$ and $d \leq 2.6$ nm for $Lam_{Sm}/c2mm$.

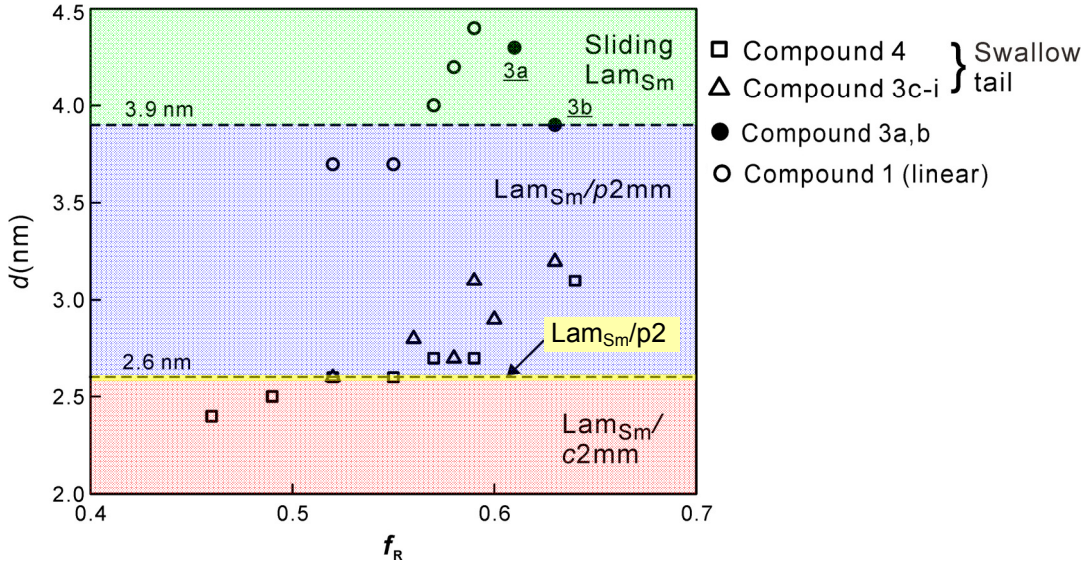


**Figure 10**. Dependence of the Lam phase type on the layer distance $d$ and the volume fraction $f_R$.

### 2.2.4 Swallow-tailed compounds with two alkyl-fluoroalkyl branches – effects of layer curvature

Compounds **7** contain a swallow-tail side-group with two long alkyl ($C_{11}H_{22}$) segments and a fluorocarbon segment of varying lengths at each end (Table 5).[18] In this series of compounds where both branches were fluorinated, the aromatic layers contain the same number of only two side-by-side lying biphenyls in thickness ($n_{wall}$ = 2, see Table 5) as observed for all other swallow tailed compounds. The absence of off-meridional reflections in the XRD patterns, the presence of an additional $Lam_N$ phase and layer distances $d > 3.95$ nm support the formation of sliding $Lam_{Sm}$ phases for compounds **7b-d**, whereas the absence of $Lam_N$, a layer distance $d < 3.95$ nm and the typical "spherulitic" texture (see Figure S2) are in line with a correlated $Lam_{Sm}$ phase for **7a**.[18] That sliding $Lam_{Sm}$ and $Lam_N$ phases could be achieved for swallow-tailed molecules (with $n_{wall}$ = only 2) by using sufficiently large chains

supports the hypothesis that layer coupling is mainly determined by the layer distance and less by the type of lateral chains (*vide supra*).

**Table 5.** Mesophases of Swallow Tailed Compounds **7** with Two Semiperfluorinated Alkyl Branches.[a, 18]

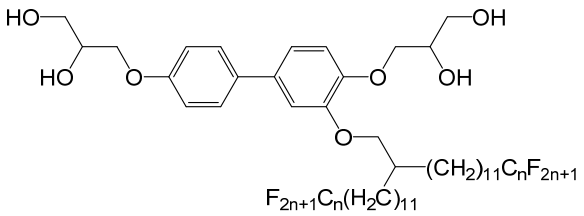


| Comp. | *n* | *T* [°C]<br>$\Delta H$ [kJ·mol$^{-1}$] | *d* /nm [b] | $f_R$ | $n_{wall}$ |
|---|---|---|---|---|---|
| **7a** | 4 | Cr 60 $Lam_{Sm}$ [c] 129 Iso<br>*16.4* *7.2* | 3.7 | 0.69 | 2.0 |
| **7b** | 6 | Cr 57 $Lam_{Sm}$ 119 $Lam_N$ 125 $Col_{rec}$/*c2mm* 131 Iso<br>*13.7* *0.2* *2.7* | 4.0 | 0.72 | 2.0 |
| **7c** | 8 | Cr 75 $Lam_{Sm}$102 $Lam_N$ 106 $Col_{rec}$/*c2mm* 132 Cub/*Ia3d* 154 Iso<br>*36.4* *1.3* *0.9* *1.1* | 4.5 | 0.74 | 2.0 |
| **7d** | 10 | Cr108 $Lam_{Sm}$ 132 $Lam_N$ 133 $Col_{rec}$/*c2mm*145 Cub/*Ia3d* 178 Iso<br>*45.3* *5.7* *1.9* *1.3* | 5.2 | 0.76 | 2.1 |

[a] for conditions and abbreviations, see Tables 1 and 3; additional abbreviation: $Col_{rec}$/*c2mm* = rectangular columnar phase with *c2mm* lattice formed by elliptical coaxial rod-bundles in a continuum of the lateral chains; [18] Cub/*Ia3d* = bicontinuous cubic phase (gyroid) formed by two networks of branched coaxial rod-bundles in the continuum of the lateral chains;[18] [b] the *d*-values and $n_{wall}$ refer to the $Lam_{Sm}$ phases; [c] based on the textural similarity with the $Lam_{Sm}$/*p2mm* of compound **1d** it is most probably $Lam_{Sm}$/*p2mm* (see Figure S2).

From Table 5 it can also be seen that at increasing temperature, compounds **7b-d** form a series of phases that are not lamellar any more. The polar and non-polar subspaces are not divided by a flat interface (zero curvature), as in the case of Lam phases, but rather by a curved one that is convex, or negative, curving to enclose the aromatic-glycerol domains. Moving from flat to curved interface we are entering the range at the top right on the phase cycle in Figure 1. The high-temperature phases displayed by compounds **7b-d** include a coaxial rod-bundle ribbon phase, $Col_{rec}$/*c2mm*, which is a rectangular columnar phase with centered lattice, and the bicontinuous cubic double gyroid phases, Cub/*Ia3d*, consisting of interpenetrating networks of branched coaxial rod-bundle columns;[18,19] these phase types replace the expected $Lam_{Iso}$ phase range.

10.1002/chem.201802050

The one thing that compounds **7b-d** have in common are two long flexible chains branching off close to the biphenyl core. At low temperature these chains have a high contribution of linear *all-trans* conformation, thus retaining the Lam phases, whereas at increased temperature the *gauche* content increases, causing overcrowding at the polar-nonpolar interface and causing it to curve. The other essential ingredient of these compounds is a sufficiently large $R_F$ segment which helps phase segregation, raising the isotropization temperature. Without such $R_F$ groups (compounds **4** and **6**), or where the $R_F$ group is too small (compound **7a**), the materials instead turn isotropic below the temperatures of the flat-curved interface transition.

## 3. Summary and Conclusions

Chain branching and fluorination were used as side chain engineering tools in directing self-assembly of rod-like bolaamphiphilic molecular cores. A special type of negatively birefringent lamellar phases with the rods arranged parallel to the layer planes (in-plane smectics) develops with growing lateral chain volume at the transition from the polygonal honeycombs with positive[12,13] to the coaxial rod-bundle type columnar phases with negative interface curvature (Figure 1).[20]

A sequence of six lamellar phases, differing in intra-layer order and inter-layer correlation of constituent molecules was found upon strengthening of layer coupling. These range from lamellar isotropic ($Lam_{Iso}$) via lamellar nematic ($Lam_N$) and positionally non-correlated (sliding) lamellar smectic ($Lam_{Sm}$) and finally lead to three different types of correlated lamellar smectic phases with *p*2*mm, p*2 and *c*2*mm* lattice (Figure 9). The AB coupling (*c*2*mm*) is favoured by steric effects between closely coupled layers. The transition from the centred *c*2*mm* to the primitive *p*2*mm* structure is attributed to an increased contribution of thermal fluctuation. If these fluctuations take place perpendicular to the layers (transverse) they favour the *p*2*mm* lattice, whereas excitation parallel to the layers (longitudinal) decreases the

10.1002/chem.201802050

coherence length of positional inter-layer coupling, thus leading to the sliding lamellar smectic phases (Figure 9). It appears that the two modes of fluctuations exclude each other, i.e., as long as there are transverse fluctuations, sliding of the layers is suppressed and the long range *p*2*mm* lattice is retained up to the transition to the isotropic liquid state. As soon as the longitudinal fluctuations become dominant, the formation of a long range lattice is inhibited and any positional correlation remains short range; the resulting sliding $Lam_{Sm}$ phase is succeeded by additional $Lam_N$ and $Lam_{Iso}$ phases on further heating, before the transition to Iso.

The strength of inter-layer coupling in the first instance decreases with increasing distance between the layers, as shown in Figure 10. The major reduction of *d* arises due to the transition from three to only two molecules in the cross section of the biphenyl+glycerol walls upon chain branching, and the reduction is further supported by a reduction in chain volume. Beside the layer distance, the strength and directionality of chain interactions is also of importance.[32,33] Swallow-tail chains have the strongest tendency to align parallel to rod-like cores (Figures S25, S26), and hence support orientational layer coupling. Perfluorinated segments obviously have a higher tendency to be arranged parallel to each other and preferentially perpendicular or tilted to the layers (Figure 7b); thus they do not significantly contribute to layer coupling. As a consequence of these effects the swallow-tailed chains (compounds **3**, **4**) provide a stronger inter-layer coupling than linear ones with the same chain volume (compounds **1**, **5**), independent of whether they are fluorinated or not. Shifting the lateral chain to a more central position (compound **2**) distorts intra-layer core packing itself and thus leads to an intrinsically reduced correlation between the rods.

Chain branching and chain fluorination are associated with the development of negative interface curvature, and its absolute value increases with rising temperature. This results in the adoption of coaxial rod-bundle columnar or cubic network phases (Figure 1) with curved interfaces and 2d or 3d lattice (compounds **7**) with increasing chain volume.[18]

Overall, this work establishes the generic phase sequence of the LC in-plane smectic phases (90° tilted smectics, Lam phases) and provides a fundamental understanding of the transition from sliding to locked types. The possibility of in-plane reorganization of the rod-like molecules in the $Lam_N$ and $Lam_{Sm}$ phases is analogous to biaxial nematic ($N_b$)[34] and biaxial SmA phases ($SmA_b$)[35] and could lead to applications in light modulators and displays.[4] Moreover, these small molecules can be considered as model systems for understanding the self-assembly of larger rigid π-conjugated molecular rods, oligomers and polymers,[24,36,37] which are known to be of importance for application in fluorescence, organic electronics and light harvesting.[6,25] For example, the molecular orientation affects the efficiency of photovoltaic cells.[38] However, rational design of molecular structures to achieve a desired mode of alignment of π-conjugated rods by side chain engineering is still in its infancy and is mainly bases on a trial-and-error approach.[26,27] In this article we provide a fundamental understanding of in-plane organization of π-conjugated rods for simple generic model compounds. The understanding of layer coupling applies also to the presently topical 2d materials ranging from graphene sheets to lamellar metallorganic frameworks and 2d polymers, where it influences their application properties.[1,3] It is also of relevance for tailoring the self-assembly of larger rod-like units, e.g. hairy-rod polymers,[39] DNA strands[10] and nanoparticles in lyotropic systems.[40]

*Acknowledgments*. This work was supported by DFG (392435074), National Natural Science Foundation of China (No. 21761132033) and EPSRC (EP_K034308 and EP_P002250). For help with synchrotron experiments we thank Prof. Nick Terrill at I22 at Diamond Light Source and Drs. O. Bikondoa, S. Brown and P. Thompson at BM28 at ESRF.

**References**

[1] a) J. Sakamoto, J. van Heijst, O. Lukin, A. D. Schlüter, *Angew. Chem. Int. Ed.* **2009**, *48*, 1030 – 1069; b) C. E. Boott, A. Nazemi, I. Manners, *Angew. Chem. Int. Ed*. **2015**, *54*,

13876 – 13894; c) Z. Xiang, D. Cao, L. Dai, *Polym. Chem*. **2015**, *6*, 1896–1911; d) X. Zhuang, Y. Mai, D. Wu, F. Zhang, X. Feng, *Adv. Mater*. **2015**, *27*, 403–427; e) F. Yang, S. Cheng, X. Zhang, X. Ren, R. Li, H. Dong, W. Hu, *Adv. Mater.* **2018**, *30*, 1702415.

[2] (a) S. Norvez, J. Simon, *Liq. Cryst.* **1993**, *14*, 1389-1395; b) P. Bassoul, J. Simon, C. Soulie, *J. Phys. Chem*. **1996**, *100*, 3131-3136; c) S. Norvez, F. G. Tournilhac, P. Bassoul, P. Herson, *Chem. Mater* **2001**, *13*, 2552-2561; d) K. Ohta, R. Higashi, M. Ikejima, I. Yamamoto, N. Kobayashi, *J. Mater. Chem*. **1998**, *8*, 1979-1991; e) A. Kosaka, T. Hikima, M. Takata, T. Someya, N. Seiki, Y. Shoji, T. Kajitani, F. Ishiwari, T. Fukushima, *Science* **2015***, 348*, 1122-1126; f) X.-S. Hou, G.-L. Zhu, L.-J. Ren, Z.-H. Huang, R.-B. Zhang, G. Ungar, L.-T. Yan, W. Wang, *J. Am. Chem. Soc.* **2018**, *140*, 1805−1811.

[3] R. Hoffmann, *Angew. Chem. Int. Ed*. **2013**, *52*, 93-103.

[4] *Handbook of Liquid Crystals*, 2nd Ed.; J. W. Goodby, P. J. Collings T. Kato, C. Tschierske, H. F. Gleeson, P. Raynes, Eds.; Wiley-VCH, Weinheim, Germany, 2014.

[5] a) G. W; Gray, J. W. G. Goodby, *Smectic Liquid Crystals*, Leonard Hill, Glasgow, 1984; b) A. J. Leadbetter, *Structural classification of liquid crystals*. In *Critical Reports on Applied Chem*istry, Vol. 22: *Thermotropic Liquid Crystals*; G. W., Gray, Ed.; Wiley: Chichester, UK, 1987; 1-27.

[6] T. Kato, M. Yoshio, T. Ichikawa, B. Soberats, H. Ohno, M. Funahashi, *Nat. Rev. Mater*. **2017**, *2*, 17001.

[7] a) J.M. Kosterlitz, D. J. Thouless, *J. Phys. C* **1973**, *6*, 1181-1203; b) P. G. DeGennes, *Symp. Faraday Soc*. **1971**, *5*, 16-24; c) B. I. Halperin, D. R. Nelson, *Phys. Rev. Lett*. **1978**, *41*, 121-124.

[8] P. L. Felgner, T. R. Gader, M. Holm, R. Roman, H. W. Chan, M. Wenz, J. P. Northrop, G.M. Ringold, M. Danielsen, *Proc. Natl. Acad. Sci. USA* **1987**, *84*, 7413-7417.

[9] J. O. Rädler, I. Koltover, T. Salditt, C. R. Safinya, *Science* **1997**, *275*, 810-814.

[10] G. Caracciolo, D. Pozzi, R. Caminiti, G. Mancini, P. Luciani, H. Amenitsch, *J. Am. Chem. Soc*. **2007**, *129*, 10092–10093.

[11] a) L. Golubovic, M. Golubovic, *Phys. Rev. Lett*. **1998**, *80*, 4341-4344; b) C. S. O'Hern T. C. Lubensky, *Phys. Rev. Lett*. **1998***, 80*, 4345-4348, c) L. Golubovic, T. C. Lubensky, C. S. O'Hern, *Phys. Rev. E* **2000**, *62*, 1069-1094.

[12] a) C. Tschierske, *Chem. Soc. Rev*. **2007**, *36*, 1930-1970; b) C. Tschierske, C. Nürnberger, H. Ebert, B. Glettner, M. Prehm, F. Liu, X. B. Zeng, G. Ungar, *Interface Focus* **2012**, *2*, 669−680; c) G. Ungar, C. Tschierske, V. Abetz, R. Holyst, M. A. Bates, F. Liu, M. Prehm, R. Kieffer, X. Zeng, M. Walker, B. Glettner, A. Zywocinski, *Adv. Funct. Mater.* **2011**, *21*, 1296–1323; d) C. Tschierske, *Angew. Chem., Int. Ed*. **2013**, *52*, 8828−8878.

[13] a) M. Kölbel, T. Beyersdorff, X. H. Cheng, C. Tschierske, J. Kain, S. Diele*, J. Am. Chem. Soc.* **2001**, *123*, 6809-6818; b) X. H. Cheng, M. Prehm, M. K. Das, J. Kain, U. Baumeister, S. Diele*,* D. Leine, A. Blume, C. Tschierske, *J. Am. Chem. Soc.* **2003**, *125*, 10977-10996; c) X.-H. Cheng, M. K. Das, U. Baumeister, S. Diele, C. Tschierske, *J. Am. Chem. Soc.* **2004**, *126*, 12930-12940; d) M. Prehm, G. Görtz, P. Bäuerle, F. Liu, X. Zeng, G. Ungar, C. Tschierske, *Angew. Chem, Int. Ed*. **2007**, *46*, 7856-7859.

[14] a) X. H. Cheng, M. K. Das, S. Diele, C. Tschierske, *Angew. Chem. Int. Ed*. **2002**, *41*, 4031-4035; b) M. Prehm, X. H. Cheng, S. Diele, M. K. Das, C. Tschierske, *J. Am. Chem. Soc*. **2002**, *124*, 12072-12073.

[15] M. Prehm, C. Enders, M. Y. Azahaee, B. Glettner, U. Baumeister, C. Tschierske, *Chem. Eur. J.*, **2008**, *14*, 6352-6368.

[16] R. Kieffer, M. Prehm, K. Pelz, U. Baumeister, F. Liu, H. Hahn, H. Lang, G. Ungar, C. Tschierske, *Soft Matter* **2009**, *5*, 1214-1227.

[17] M. Prehm, F. Liu, U. Baumeister, X. Zeng, G. Ungar, C. Tschierske, *Angew. Chem, Int. Ed*. **2007**, *46*, 7972-7975.

[18] a) F. Liu, M. Prehm, X. Zeng, C. Tschierske, G. Ungar, *J. Am. Chem. Soc*. **2014**, *136*, 6846-6849.

[19] X. Zeng, M. Prehm, G. Ungar, C. Tschierske, F. Liu, *Angew. Chem. Int. Ed*. **2016**, *55*, 8324-8327.

[20] (a) M. Prehm, F. Liu, X. Zeng, G. Ungar, C. Tschierske, *J. Am. Chem. Soc.* **2008***, 130*, 14922–14923; b) M. Prehm, F. Liu, X. Zeng, G. Ungar, C. Tschierske, *J. Am. Chem. Soc*. **2011**, *133*, 4906-4916.

[21] a) N. M. Patel, M. R. Dodge, M. H. Zhu, R. G. Petschek, C. Rosenblatt, M. Prehm, C. Tschierske, *Phys. Rev. Lett*. **2004**, *92*, 015501; b) N. M. Patel, I. M. Syed, C. Rosenblatt, M. Prehm, C. Tschierske, *Liq. Cryst.* **2005**, *32*, 55-61; c) N. Chattham, C.

Zhu, X.-H. Cheng, J. Limtrakul, C. Tschierske, J. E. Maclennan, N. A. Clark, *Soft Matter* **2011**, *7*, 9978–9982.

[22] M. Prehm, S. Diele, M. K. Das C. Tschierske, *J. Am. Chem. Soc*. **2003**, *125*, 614-615.

[23] a) C. Tschierske, *Top. Curr. Chem.* **2012**, *318*, 1–108; b) M. P. Krafft, J. G. Riess, *Chem. Rev*. **2009,** *109,* 1714–1792.

[24] Y. Xiao, D. Zeng, L. M. Mazur, A. Castiglioneo E. Lacaze, B. Heinrich, B. Donnio, D. Kreher, A.-J. Attias, J. C. Ribierre, F. Mathevet, *Polymer Journal*, **2017**, 49, 31–39.

[25] a) M. O'Neill, S. M. Kelly, *Adv.Mater*. **2011**, *23*, 566-584; b) Q. Li, *Self-organized Organic Semiconductors. From Materials to Device Applications*, Wiley, 2011, Hoboken, NJ; c) A. Lützen in *Bottom-Up Self-Organization in Supramolecular Soft Matter*, C. Müller, S. C. Parisi, Eds. *Springer, Series in Matereials Science* 217, Springer, Cham, 2015, pp. 195-236; d) M. Gsänger, D. Bialas, L. Huang.; M. Stolte, F. Würthner, *Adv. Mater*. **2016**, *28*, 3615–3645.

[26] a) I. Osaka, R. D. McCullough, *Acc. Chem. Res*. **2008**, *41*, 1202–1214; b) J. Mei, Z. Bao, *Chem. Mater*. **2014**, *26*, 604-615; c) T. Lei, J.-Y. Wang, J. Pei, *Chem. Mater*. 2014, 26, 594-603; d) D. P. McMahon, A. Troisi, *ChemPhysChem* **2010**, *11*, 2067 – 2074; d) I. Kang, H.-J. Yun, D. S. Chung, S.-K. Kwon, Y.-H. Kim, *J. Am. Chem. Soc*. **2013** *135*, 14896–14899; e) H. Li, J. Choi, T. Nakanishi, *Langmuir,* **2013**, *29*, 5394-5406; f) B. Fu, J. Baltazar, A. R. Sankar, P-H. Chu, S. Zhang, D.M. Collard, E. Reichmanis, *Adv. Funct. Mater.* **2014**, *24*, 3734–3744; g) Z.-G. Zhang, Y. Li, *Sci. China Chem*. **2015**, *58*, 192-209; h) A. Mavrinskiy, C. B. Nielsen, J. R. Reynolds, K. Müllen, W. Pisula, *Chem. Mater*. **2011**, *23*, 1939–1945; i) J. Rivnay, S. C. B. Mannsfeld, C. E. Miller, A. Salleo, M. F. Toney, *Chem. Rev*. **2012**, *112*, 5488−5519.

[27] J. Mei, D. H. Kim, A. L. Ayzner, M. F. Toney, Z. Bao, *J. Am. Chem. Soc*. **2011***, 133*, 20130–20133.

[28] All compounds were prepared from racemic materials and represent mixtures of two diastereomers in their racemic forms. Due to the separation of the stereogenic centers by the rod-like units it is assumed that there is only a weak interaction between them so that the diastereomers are formed in almost equal amounts and that there is no significant separation of the diastereomers during chromatography. Compounds **3** represent even more complex mixtures, as they involve three stereogenic centers, all in the racemic form.

[29] a) N. Miyaura, T. Yanagi, A. Suzuki, *Synth. Commun.* **1981**, *11*, 513-519; b) M.; Hird, G. W. Gray, K. J. Toyne, *Mol. Cryst. Liq. Cryst.* **1991**, *206*, 187-204; c) N. Miyaura, A. Suzuki, *Chem. Rev.* **1995**, *95*, 2457-2483.

[30] A. Immirzi, B. *Acta Cryst. Sect. A* **1977**, *33*, 216-218.

[31] K. C. Chu, W. L. McMillan, *Physical Review A*, **1977**, *15*, 1181-1187.

[32] A. J. Cruz-Cabeza, J. Bernstein, *Chem. Rev*. **2014**, *114*, 2170-2191.

[33] J. P.; Wagner, P. R. *Angew. Chem. Int. Ed.* **2015**, *54*, 12274-12296.

[34] a) J. Freiser, *Phys. Rev. Lett.* **1970**, *24*, 1041–1043; b) C. Tschierske, D. J. Photinos, *J. Mater. Chem*., **2010**, *20*, 4263–4294.

[35] a) H. R. Brand, P. E. Cladis, H. Pleiner, *Macromolecules* **1992**, *25*, 7223-7226 ; b) H.; Leube, H. Finkelmann, *Makromol. Chem*. **1991**, *192*, 1317-1328 ; c) T. Hegmann, J. Kain, G. Pelzl, S. Diele, C. Tschierske, *Angew. Chem., Int. Ed*. **2001**, *40*, 887-890.

[36] a) R. Stepanyan, A. Subbotin, M. Knaapila, O. Ikkala, G. ten Brinke, *Macromolecules* **2003,** *36,* 3758-3763; b) X.-Q. Liu, J. Wang, S. Yang, E.-Q. Chen, *ACS Macro Lett*. **2014**, *3*, 834−838; c) H. S. Marsh, E. Jankowski, A. Jayaraman, *Macromolecules* **2014**, *47*, 2736−2747.

[37] T. Kajitani, H. Onouchi, S. Sakurai, K. Nagai, K. Okoshi, K. Onitsuka, E. Yashima, *J. Am. Chem. Soc*. **2011**, *133*, 9156–9159.

[38] L. Yang, S. Zhang, C. He, J. Zhang, Y. Yang, J. Zhu, Y. Cui, W. Zhao, H. Zhang, Y. Zhang, Z. Wei, J. Hou, *Chem. Mater*. **2018**, *30*, 2129−2134.

[39] a) M. Knaapila, R. Stepanyan, B. P. Lyons, M. Torkkeli, A. P. Monkam, *Adv. Funct. Mater*. **2006**, *16*, 599-609; b) K. Fu, N. Sekine, M. Sone, M. Tokita, J. Watanabe, *Polymer J*. **2002**, *34*, 291-297; c) B. Carbonnier, T. Pakula, D. A. M. Egbe, *J. Mater. Chem*. **2005**, *15*, 880-890; d) P. Riala, A. Andreopoulou, J. Kallitsis, A. Gitsas, G. Floudas, *Polymer* **2006**, *47*, 7241-7250; e) B. Carbonnier, A. K. Andreopoulou, T. Pakula J. K. Kallitis, *Macromol. Chem. Phys*., 2005, **206**, 66-76; Shi, H.; Zhao, Y.; Dong, X.; Zhoua, Y.; Wang, D. Frustrated crystallisation and hierarchical self-assembly behaviour of comb-like polymers. *Chem. Soc. Rev.,* 2013, **42**, 2075-2099;

[40] a) L. He, L. Zhang, Y. Ye, H. Liang, *J. Phys. Chem. B* **2010,** *114,* 7189–7200; b) R. L. Marson, T. D. Nguyen, S. C. Glotzer, *MRS Communications* **2015**, *5*, 397–406.

10.1002/chem.201802050